Optics Communications 458 (2020) 124680

Contents lists available at ScienceDirect

Optics Communications

journal homepage: www.elsevier.com/locate/optcom

# Intensity noise self-suppression in a high-efficiency doubly resonant sum frequency mixing red laser

Wei Tan [a], Weiguang Ma [b,c], Zhaojun Liu [a,*], Xiaojuan Yan [b,c], Xiaodong Qiu [d], Xingyu Zhang [a]

[a] School of Information Science and Engineering, and Shandong Provincial Key Laboratory of Laser Technology and Application, Shandong University, 266237 Qingdao, China

[b] Institute of Laser Spectroscopy, State Key Laboratory of Quantum Optics and Quantum Optics Devices, Shanxi University, 030006 Taiyuan, China

[c] Collaborative Innovation Center of Extreme Optics, Shanxi University, 030006 Taiyuan, China

[d] Department of Physics, Collaborative Innovation Center for Optoelectronic Semiconductors and Efficient Devices, and Jiujiang Research Institute, Xiamen University, 361005 Xiamen, China

ARTICLE INFO

*Keywords:*
High-efficiency
Low intensity noise
Sum frequency mixing
Cavity enhancement
Laser

ABSTRACT

A doubly resonant sum frequency mixing laser at 636 nm with a maximum output power of 637 mW is demonstrated. The conversion efficiency of signal laser reaches 93% by optimizing the sum frequency mixing setup. Based on this high conversion efficiency, we realize the intensity noise self-suppression effect. Experimental results show that even the power fluctuation of pump power was modulated up to 7.8%, the power stability of 636 nm laser kept under 0.6% The simulation results based on the exact solution of the coupled wave equations and cavity enhancement theory can explain the reason and property of the intensity noise self-suppression. Our results may find potential applications in the frequency conversion of the quantum squeezed states, imaging and cold atom physics.

## 1. Introduction

Sum frequency mixing (SFM) technology plays an important role in varieties of applications, e.g. laser generation with new wavelength, highly efficient single photon detection, long distance quantum keys distribution, quantum enhancements of spectroscopy, frequency conversion of the quantum squeezed states, imaging, and artificial beacon [1–8]. In these applications, low intensity noise is highly desirable under different conditions.

Active and positive methods have been massively investigated to suppress the laser intensity noise in different types of lasers [9–14]. Generally, the intensity noises of the SFM laser are partly resulted from the fundamental lasers. Thus, suppressing the intensity noise of the fundamental lasers is necessary. Apart from this, the thermal effect is another main problem. For a single passing SFM setup, thermal effects in the nonlinear crystal will lead to deteriorated overlapping between the two fundamental lasers and variation of the focus parameters, so that both the single pass conversion efficiency of the fundamental lasers and the output laser power will fluctuate. For the external cavity enhanced SFM, including the singly and doubly wavelength resonating schemes, besides the deteriorated overlapping and variation of the focus parameters, the coupling efficiency is also affected by the thermal effects. Therefore, the intra-cavity fundamental laser intensity and the total conversion efficiency will be unstable. Although a Peltier and a well-designed oven could be helpful to reduce the heat in nonlinear crystal, the inhomogeneous thermal effects cannot be eliminated thoroughly [15–17]. Meanwhile, frequency locking stability also affects the power stability of SFM laser. However, frequency locking cannot sweep the power fluctuation induced by the thermal effects.

Fortunately, in a cavity enhanced SFM setup, the SFM output power will be insensitive to the fundamental laser power when one of the fundamental lasers gets the maximum conversion efficiency [18]. No active feedback system is needed to suppress the SFM laser fluctuation in this scheme. Therefore, the SFM laser intensity noise is suppressed by the SFM setup itself, which is called intensity self-suppression in this manuscript. However, it is not easy to realize the near-unit conversion efficiency of a fundamental laser with hundred-milli-watt power levels. In 2004, Marius A. Albota and Franco N. C. Wong reported a high efficiency SFM with single photon level signal laser whose conversion efficiency was 93% based on singly resonant SFM [19]. Some other researchers also reported high efficiency SFM, but the input signal powers were several milli-watts [20–22]. Doubly resonant SFM could furtherly improve the conversion efficiency of the fundamental lasers, and even a low efficient nonlinear crystal could be applied to generate SFM laser [18]. An over 100 μW continuous-wave ultraviolet radiation at 370 nm was generated in a lithium iodate crystal and one of the fundamental lasers only owned 8 mW output power [23]. When the

* Corresponding author.
*E-mail address:* zhaojunliu@sdu.edu.cn (Z. Liu).

https://doi.org/10.1016/j.optcom.2019.124680
Received 5 July 2019; Received in revised form 24 September 2019; Accepted 30 September 2019
Available online 3 October 2019

powers of fundamental lasers are in the same level e.g. hundreds of milli-watts, the near-unit conversion efficiency is difficult to reach. In 1998, Joseph D. Vance, etc, reported a 400 mW 589 nm laser with optical conversion efficiency of 60% [24]. In 2003, the Air Force Research Laboratory developed a 20 W sodium beacon laser at 589 nm by mixing two high power injection-locked Nd:YAG lasers, and the conversion efficiency of the 1319 nm fundamental laser was 57% [7]. Although they improve the output power of 589 nm laser to 50 W 2 years later, the conversion efficiency decreased to 37% [25]. In 2008, Emmanuel Mimoun, etc. reported a 589 nm laser based on SFM [26]. The output power of 589 nm laser was near 800 mW, and the conversion efficiency of the 1319 nm fundamental laser was 90%. In this paper, the small signal approximation was applied to design the SFM setup, which was not precise to describe the high efficiency doubly resonant SFM scheme. In 2019, Dismas K. Choge, etc. reported a maximum orange laser output power of 129 mW corresponding the conversion efficiency of 65% [27]. In order to realize a high conversion efficiency of a high-power fundamental laser, the main parameters of an SFM setup should be carefully optimized.

In this manuscript, we construct a low intensity noise 636 nm laser with a maximum output power of 637 mW based on highly efficient doubly resonant SFM. The conversion efficiency of input signal laser reaches 93% with input power of 275 mW. Based on the high stability frequency locking and mainly the high efficiency SFM, the intensity noise of SFM laser is suppressed. The long-term output power stability and short-term output laser intensity noise are both measured in the experiment. The results indicate, under this high conversion efficiency, we realize the intensity noise self-suppression effect. Even with the power fluctuation of pump power being modulated up to 7.8%, the power stability of 636 nm laser keeps to 0.6%. A theoretical simulation based on the coupled wave equations and cavity enhancement theory is applied to explain the intensity noise self-suppression.

## 2. Theoretical model of high power SFM laser

When the conversion efficiency of both the fundamental lasers are too high to ignore, the exact solution of the coupled wave equations should be considered. To get the exact solution, the traditional coupled wave equations could be transformed to [18,28–30]

$$\begin{cases} \dfrac{du_1}{d\varsigma} = u_2 u_3 \sin\beta(\mathrm{z}) \\ \dfrac{du_2}{d\varsigma} = u_1 u_3 \sin\beta(\mathrm{z}) \\ \dfrac{du_3}{d\varsigma} = u_2 u_1 \sin\beta(\mathrm{z}) \\ \dfrac{d\beta}{d\varsigma} = \dfrac{\cos\beta(\mathrm{z})}{\sin\beta(\mathrm{z})}\left(\dfrac{d}{d\varsigma}\ln u_1 u_2 u_3\right) \end{cases} . \tag{1}$$

In these equations, the variables are defined as

$$\begin{cases} u_1 = \rho_1\sqrt{\dfrac{n_1\lambda_1}{4\pi}} \\ u_2 = \rho_2\sqrt{\dfrac{n_2\lambda_2}{4\pi}} \\ u_3 = \rho_3\sqrt{\dfrac{n_3\lambda_3}{4\pi}} \\ \varsigma = \dfrac{z}{\sqrt{\frac{n_1 n_2 n_3 \lambda_1 \lambda_2 \lambda_3}{64\pi^3}}} \end{cases} , \tag{2}$$

in which, $\rho$ is the amplitude of the electric fields without phase, $n$ is the refraction index of the nonlinear crystal, $\lambda$ is the wavelength of the three waves, and the subscript $i = 1, 2, 3$ refer to the pump, signal and SFM, respectively. $u_i$ is a new electric amplitude of the three waves. $\varsigma$ is defined as an interaction factor and $z$ is the length of the nonlinear crystal. In Eq. (1), the $\beta = \varphi_1(z) + \varphi_2(z) - \varphi_3(z) + \Delta k z$, where $\varphi(z)$ is the phase of the three waves and $\Delta k = k_1 + k_2 - k_3$ is the phase mismatch value.

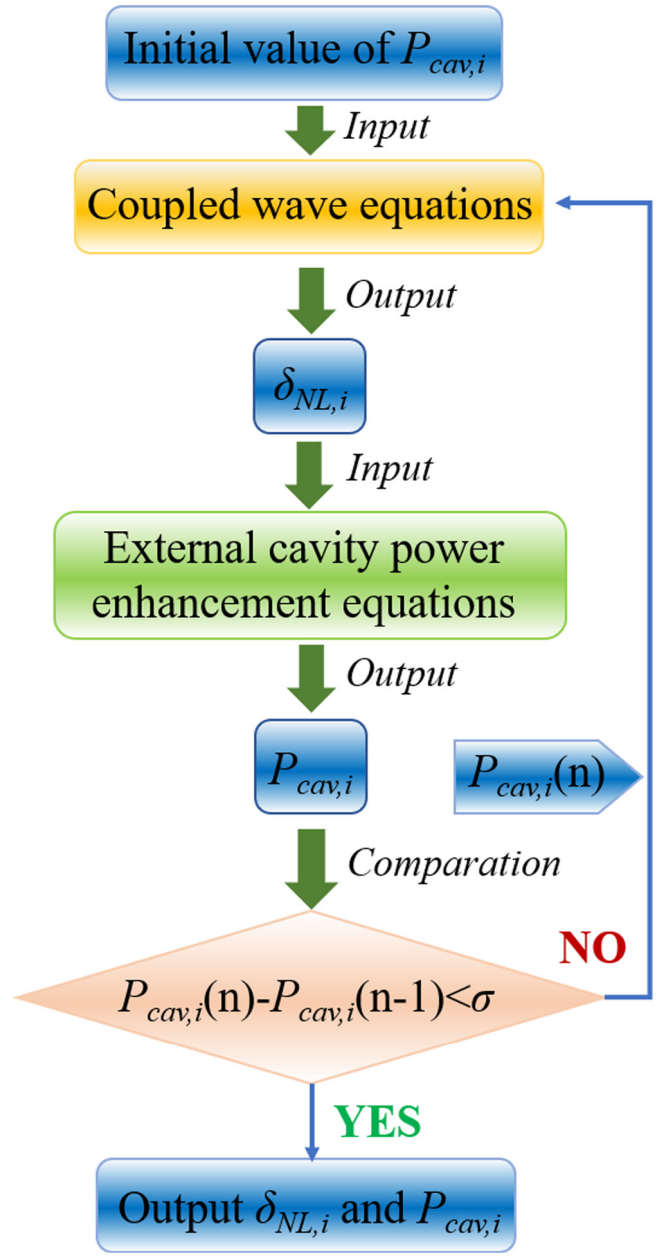


**Fig. 1.** The flow chart of iterative calculation.

If the power of the wave at $\omega_1$ is higher than that of $\omega_2$, this new coupled wave equations could be written in an elliptic integration form as,

$$\begin{cases} u_1^2 = m_1 - m_2 sn^2[m_1^{1/2}\varsigma, \dfrac{m_2}{m_1}] \\ u_2^2 = m_2 - m_2 sn^2[m_1^{1/2}\varsigma, \dfrac{m_2}{m_1}] \\ u_3^2 = m_2 sn^2[m_1^{1/2}\varsigma, \dfrac{m_2}{m_1}] \end{cases} , \tag{3}$$

in which

$$\begin{cases} m_1 = u_1^2 + u_3^2 \\ m_2 = u_2^2 + u_3^2 \\ m_3 = u_1^2 - u_2^2 \end{cases} . \tag{4}$$

It is available to calculate the electric amplitude of the fundamental waves, $u_1$ and $u_2$, by software e.g. MATLAB [27]. Then the nonlinear power loss of each fundamental lasers, $\delta_{NL,i}$, could be derived out and

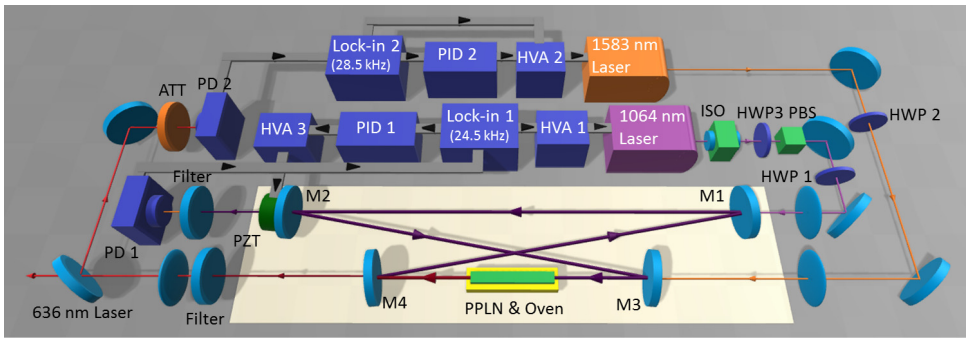


**Fig. 2.** Experimental setup of the doubly resonant SFM. ISO, optical isolator; HWP, half wave plate; PBS, polarized beam splitter; PD, photodiode; ATT, attenuator; HVA, high voltage amplifier; Lock-in, lock in amplifier; PID, Proportion Integration Differentiation circuits; PZT, Piezo-electric Transducer.

average laser power $P$ can be calculated from

$$P = \frac{1}{2} nc\varepsilon_0 \rho^2 \left(2\pi r^2\right), \tag{5}$$

where the $c$ is the light speed, $\varepsilon_0$ is the vacuum dielectric constant, and $r$ is the beam waist radius in the crystal.

In a cavity enhanced SFM setup, the intra-cavity fundamental laser power, $P_{cav,i}$, can be calculated by the external cavity power enhancement equation, which is

$$P_{cav,i} = \frac{k_i \left(1 - R_{in,i}\right) P_{in,i}}{\left(1 - \sqrt{R_{in,i}\left(1 - \delta_{L,i}\right)\left(1 - \delta_{NL,i}\right)}\right)^2}. \tag{6}$$

Here, $k_i$ is the mode coupling efficiency, and $R_{in,i}$ is the reflectivity of the input coupler. $P_{in,i}$ is the incident fundamental laser power. $\delta_{L,i}$ is the linear loss and $\delta_{NL,i}$ is the nonlinear loss. $i$ refers 1 and 2 corresponding to the pump and signal waves. Since the $P_{cav,i}$ is a function of $\delta_{NL,i}$, an iterative calculation between coupled wave equations and the external cavity power enhancement equation is needed to calculate the SFM output power. The iterative process is shown in Fig. 1. The initial value of $P_{cav,i}(0)$ is $P_{in,i}\cdot(1-R_{in,i})$, and by using Eqs. (1)–(4) can calculate the nonlinear loss of the pump and signal lasers. Then $\delta_{NL,s}$ and $\delta_{NL,p}$ are substituted to Eq. (6) to calculate new intracavity pump and signal power $P_{cav,i}(1)$. We compare the $P_{cav,i}(1)$ with $P_{cav,i}(0)$ and call on $\sigma$ as an error for control iterative process. If the difference between $P_{cav,i}(1)$ and $P_{cav,i}(0)$ is bigger than the $\sigma$, $P_{cav,i}(1)$ will be substituted to the coupled wave equations and perform a new round calculation. When the difference between $P_{cav,i}$(n) and $P_{cav,i}(n-1)$ is smaller than the $\sigma$, the iterative process outputs the results of $P_{cav,i}$ and $\delta_{NL,i}$. The cavity enhanced conversion efficiency of the signal photon could be achieved, which is

$$\eta_2^{ce} = \frac{N_3}{N_{in,2}} = \frac{P_3/n_3\omega_3}{P_{in,2}/n_2\omega_2} = \frac{\delta_{NL,2}\cdot P_{cav,2}}{P_{in,2}}, \tag{7}$$

in which $N_i$ refers to the photon number, $N_{in,2}$ is the photon number of the input signal wave. Finally, the SFM output power, $P_3$, could be derived out based on Eq. (6).

## 3. Experimental setup and results

In the SFM system, 1583 nm laser and 1064 nm laser act as the signal laser and pump laser, respectively. The experimental setup of doubly resonant SFM is shown in Fig. 2 which is similar with our previous work [21]. The narrow linewidth solid-state pump laser and fiber signal laser whose linewidth are both in kHz-level were coupled into the SFM cavity from mirror M1, and mirror M3, respectively. Two plane mirrors, M1 and M2, two plane-concave mirrors with curvature radius of 100 mm, M3 and M4, and a 25 mm long MgO doped periodically poled lithium niobate (MgO:PPLN) crystal all together constructed the main structure of the SFM cavity. M1 was highly reflective for signal laser and partial reflective of 94.7% for pump laser, and M3 was highly reflective for pump laser and partial reflective of 52.1% for signal laser. The M2 and M4 are both highly reflective for the fundamental lasers and highly transmissive for SFM laser. The total length of this cavity was 691 mm so that the beam waists in the crystal center of pump and signal lasers were 32 μm and 39 μm, respectively.

Low frequency modulation technique was used to resonating the fundamental lasers and the cavity. Lock in amplifier (Lock-in) 1 modified the pump frequency by the high voltage amplifier (HVA) 1, then demodulated the error signal from the 1064 nm cavity transmission detected by photodiode (PD) 1. Proportion Integration Differentiation (PID) circuits modified the error signal and sent it to the HVA 2 to lock the SFM cavity to the pump laser. When the pump laser is resonating in the cavity, the signal laser is depleted to a low level. Therefore, the cavity mode of signal laser is too weak to be used to demodulate a high signal to noise ratio (SNR) error for a stable frequency locking. Hence, an indirect frequency locking scheme was applied in this work. Theoretically the peak of signal cavity mode corresponds to the maximum output intensity of 636 nm laser, and the frequency modulation of the signal laser transfers to the 636 nm laser. So it is feasible to extract an error signal from the 636 nm wave to resonate the 1583 nm laser and the SFM cavity. In our experiment, the output frequency of 1583 nm laser is modulated by Lock-in 2 and the HVA 3. A small part of 636 nm laser reflected from the main optical path was received by a silicon-based PD 2, then the signal of PD 2 is delivered to Lock-in 2 for mixing with the modulation signal and achieving the error signal. Filtered by the PID 2, this error signal is feedback to the PZT in the 1583 nm laser to realize the resonating. Furtherly the SNR of the error signal could be optimized easily by adjusting the intensity of the reflected 636 nm laser. By this resonating scheme, the intensity noise caused by the frequency locking progress could be suppressed to a quite low level.

In this work, we also optimized the overlapping between the 1064 nm and 1583 nm lasers and the mode coupling of the fundamental lasers to the SFM cavity. As a result, the single-pass conversion efficiency of the fundamental lasers is increased from the parameters in Ref. [21], which is helpful to get a maximum conversion efficiency of a hundred-milli-watt level signal laser.

When the 1583 nm and 1064 nm lasers were both resonating with the SFM cavity, the input power of 1583 nm laser was fixed to the available maximum of 275 mW and the input power of 1064 nm laser was tuned from 42 mW to 942 mW. In this experiment, the output power of SFM laser at 636 nm was measured as a function of the input pump power as shown in Fig. 3. The simulation result based on our theoretical model is plotted in solid line in Fig. 3. The parameters of this simulation are from the ref 21. When the input pump power reached the available maximum power of 942 mW, the output power of 636 nm laser was 637 mW. Thus, the conversion efficiency of the signal laser can be calculated as 93%. Since the hundred-milli-watt level intra-cavity 1583 nm laser depletes the pump power heavily, the intra-cavity pump power is not a linear function of the input pump power as shown by the dash line in Fig. 3.

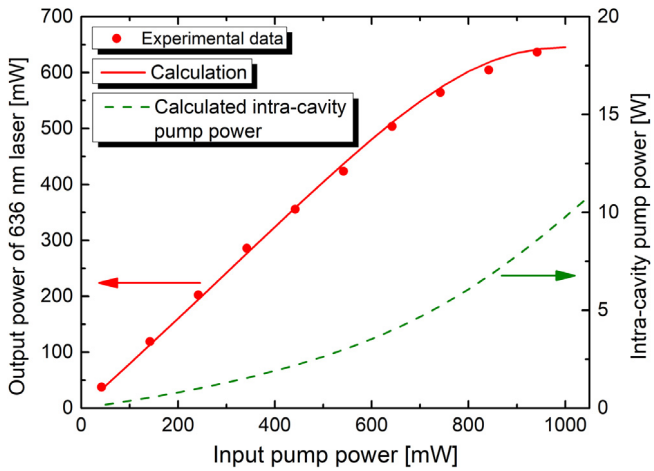


**Fig. 3.** Output power of 636 nm laser and intra-cavity pump power as functions of input pump power when the input 1583 nm laser power is 275 mW.

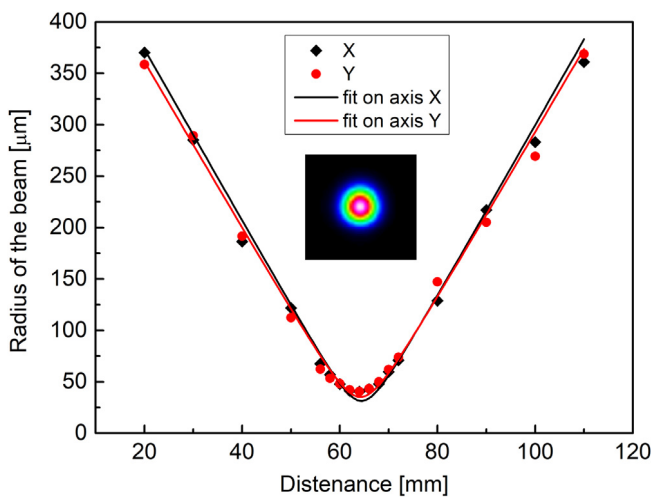


**Fig. 4.** Beam quality of 636 nm laser with output power of 637 mW.

The beam quality of the 636 nm light field at the maximum output power was measured by a beam quality analyzer (BP209-VIS, Thorlabs). The $M_x^2$ and $M_y^2$ were both 1.09, as shown in Fig. 4. Considering linewidth of the pump and signal lasers are both in kHz-level and the doubly resonating is stable, the 636 nm laser is also single frequency and narrow linewidth. However, because of the frequency noise induced by the mechanical vibration and temperature fluctuation, the linewidth of 636 nm laser is expected under hundred kHz.

In the experiments, we also measured the long-term power stability of the output 636 nm laser. The experimental results show that the SFM laser remains stable even the fundamental laser power fluctuated. The laser intensities of the 636 nm laser and fundamental lasers were monitored by three photodetectors. Since the SFM laser was generated directly by the intra-cavity high intensity fundamental lasers, the cavity transmissions of the 1064 nm and 1583 nm lasers were monitored instead of the input laser intensity. In the experiment, a Silica-based photodiode with a bandwidth of 170 MHz was employed to monitor the SFM laser, and two InGaAs-based photodiodes with bandwidths of 775 kHz were used for the fundamental lasers. The experimental data were recorded by a data acquisition card (NI, USB 6351, USA) with an acquisition sampling rate of 4 date point per second. In order to compare the noise levels of the three lasers, variable attenuators were inserted in front of each photodiode to control all three output DC amplitudes to about 1.5 V. The results are displayed in Fig. 5.

The power fluctuation of the 636 nm laser in 1 h is 1.8% which is the lowest among the three lasers. While the fluctuation of the pump and signal lasers are 4.5% and 7.2%, respectively. The fluctuations of the intra-cavity lasers are all higher than those of the input lasers because of the SFM. We also measured the fluctuation of the signal laser when the pump laser was blocked from the SFM cavity, and the result was 2.5%. This lower fluctuation indicates the thermal effects induced by the intra-cavity signal laser could be ignored. In fact, an inhomogeneous thermal effect in the crystal rises quickly when the pump laser is resonating in the SFM cavity. When the signal laser is blocked, the intensity fluctuation of intra-cavity pump laser is 4.4%. The thermal effects change the coupling efficiency and deteriorate the overlapping of the two fundamental laser fields, so that the intra-cavity fundamental laser power fluctuation is increased. Since in the cavity the pump power is higher than the signal power, the relative fluctuation of the pump laser is smaller than that of the signal laser. The inset shows the Allan variances of the long-term power fluctuation data in Fig. 5. The Allan variance of the 636 nm laser has the lowest noise level than others in all averaging times, which indicates the intensity self-suppression is operational. A bump stands at averaging time around 10 s for the light fields except 636 nm laser, which is attributed to the temperature variation of the crystal.

Like the long-term power stability of the three lasers, the short-term intensity noise of the lasers is also affected by the SFM process. In order to evaluate the short-term noise of the system, the light intensity of the three light fields detected by the photodiodes were sent to a spectrum analyzer (Rohde–Schwarz, FSW-13, Germany) to assess their noise levels. The output signals of the photodiodes were adjusted to the same DC voltage (1.5 V) to ensure the intensity noise comparable. A high pass filter with a corner frequency of 0.2 Hz is employed to filter out the DC components to protect the spectrum analyzer. Fig. 6 shows the noises of the four laser fields from 1 kHz up to 1 MHz. For comparison, the inset shows the noise level for each photodiode and the background noise level of the spectrum analyzer. As shown by the results, below 5 kHz, the intensity noise of 636 nm laser is the lowest, and the noise level is highest for 1583 nm laser. This result is coincidence with the long-term situation. Peaks in the high frequency range are the modulation frequency patterns at 28.5 kHz and 24.5 kHz and the relaxation oscillation noises of the 1583 nm laser at 500 kHz and of 1064 nm laser at 400 kHz. As the intensity noise in high frequency range shows, the intensity noise of the SFM laser is not suppressed, which indicates the intensity noise self-suppression effect could only be valid for the power fluctuation at low frequency.

In order to find the relationship of the amplitude fluctuations of the three light fields, the intra-cavity pump power was modulated with a relative amplitude variation of 7.8% and frequency of 30 Hz by inserting an acousto-optic modulator (AOM) in the input path of the pump laser. Accordingly, the powers of the cavity transmitted 1583 nm and the 636 nm light fields experienced intensity modulations with relative amplitude variations of 11.4% and 0.6%, respectively, as shown in Fig. 7. Higher pump power modulation amplitude was not performed because of the rf-output limit in the AOM. Since the intensity modulation frequency is too fast to record the temperature variation of the crystal, the relative intensity variation ratio between the 1583 nm laser and 1064 nm laser is smaller than the results in Fig. 5. Opposite variation phase between the pump and signal lasers is evident. Based on the experimental parameters, we simulated the normalized power of the 636 nm light field (normalized with respect to the maximum output power of the 636 nm laser converted by the incident signal laser) and the normalized transmitted power of signal field (normalized with respect to the input signal power) as functions of the intra-cavity pump power as shown in the inset. The experiments were performed in the rectangle shadow region where the output power of 636 nm laser is around its maximum. The simulations verify that, near the maximum conversion efficiency, the variation of the pump power can cause a notable power variation of the signal field but can

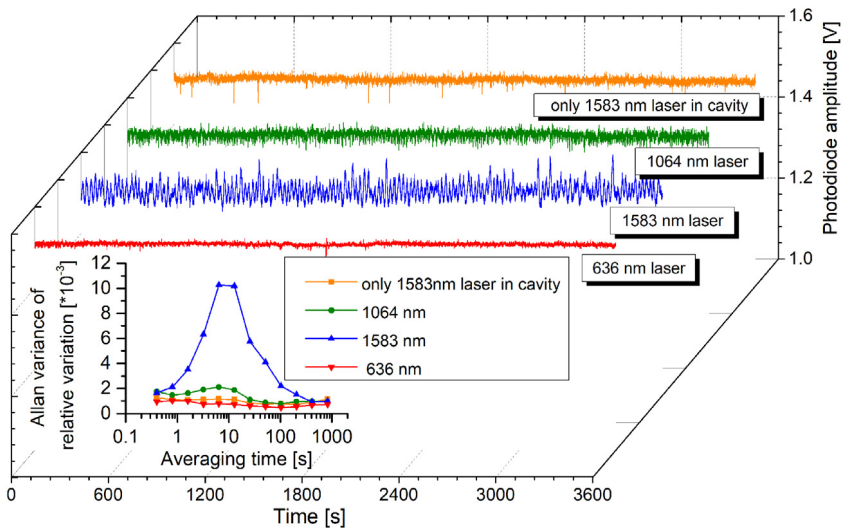


**Fig. 5.** Long-term power relative variation of four kinds of laser fields in 1 h, inset shows the corresponding Allan variances.

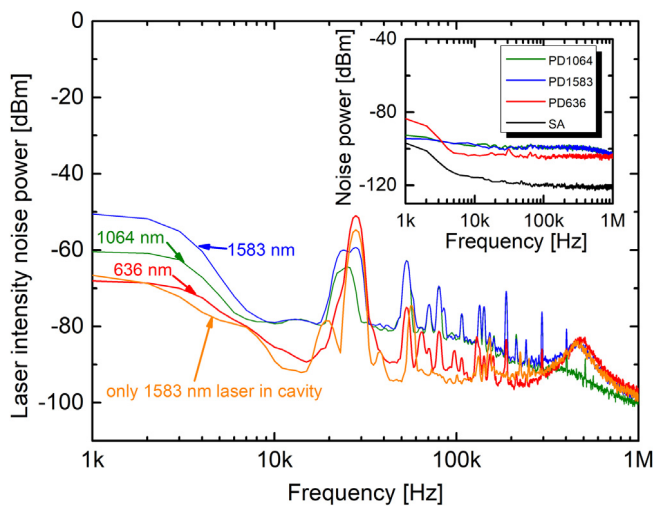


**Fig. 6.** The short-term intensity noise of the four light fields. Inset shows the intrinsic noise of the photodiodes (PD1064, PD1583 and PD636) and the spectrum analyzer (SA).

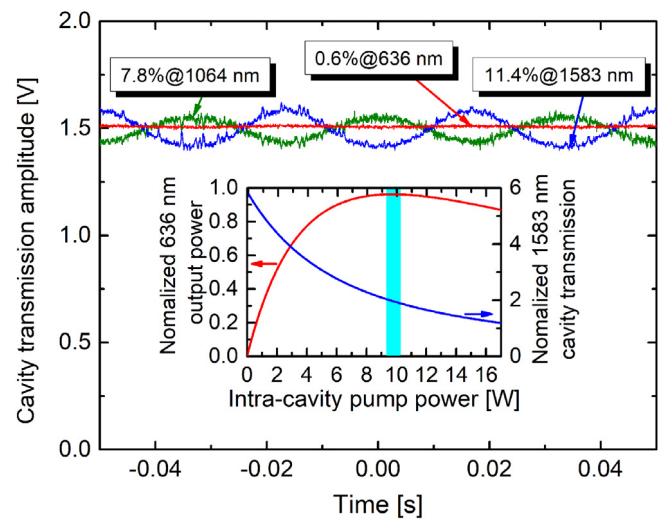


**Fig. 7.** The variation of the cavity transmission intensity of the 1064 nm, 1583 nm, and 636 nm light fields when the power of the intra-cavity 1064 nm light field is modulated by a sinusoidal voltage with a relative modulation amplitude of 7.8%. Inset shows the theoretical simulations of the normalized 636 nm output power and the normalized 1583 nm cavity transmission as functions of the intra-cavity pump power.

only lead to a minute variation of the SFM field. The reason is, when the pump power increases from the maximum SFM output condition, nonlinear loss of the signal laser rises. However, the intra-cavity signal laser decreases because of the impedance mismatch caused by the rising nonlinear loss. As shown in the experimental and theoretical results, signal power decreasing rate is higher than the increasing rate of pump laser. This means a part of signal power was extruded from the cavity, while the conversion efficiency of residual signal laser in cavity increased. Overall, the SFM laser power almost remains the same value automatically, meanwhile the intensity noise is suppressed by the SFM setup.

## 4. Conclusion

Based on doubly resonant sum frequency mixing, a 636 nm laser with output power of 637 mW was demonstrated. Conversion efficiency of the 275 mW signal laser was 93%, while the 1064 nm pump power was 942 mW. By measuring the long-term power stability and the short-term intensity noise of the three laser fields, we found the intensity noise self-suppression of the SFM laser. According to the exact solution of the three wave coupled equations and cavity enhancement theory, the theoretical simulation results show a stable output power when the conversion efficiency of signal laser reaches the maximum. Also, a power modulation experiment was performed to measure the intensity variation ratio of the three laser fields, and the results prove that the SFM output laser has a quite stable output power even the power of signal laser fluctuated by 11.4% in our setup. This experiment shows that the highly efficient SFM is the main reason of the low intensity noise SFM laser, although the frequency locking is quite stable either. Additionally, the optimized SFM crystal temperature is also necessary. This condition allows the thermal effects change the crystal temperature in a small range, which cannot vary the conversion efficiency heavily. With the characters of immune of thermal effect and low demand on frequency locking, this intensity noise self-suppression effect could be a useful method in designing low intensity noise lasers.

## Acknowledgments

This work was supported by the National Natural Science Foundation of China (Grants 11804192, 61875107, 61675122, 11704263),

China Postdoctoral Science Foundation (Grant 2018M642651), the Joint Foundation from Ministry of Education (Grants 6141A02022413, 6141A02022421), Young Scholars Program of Shandong University (Grant 2016WLJH13), and The Fundamental Research Funds of Shandong University (Grants 2018JCG02, 2017JC023).

## References

[1] P.G. Wigley, Q. Zhang, E. Miesak, G.J. Dixon, High-power 467 nm passively locked signal-resonant sum-frequency laser, Opt. Lett. 20 (24) (1995) 2496–2498.
[2] A. Samblowski, C. E.Vollmer, C. Baune, J. Fiurasek, R. Schnabel, Weak-signal conversion from 1550 to 532 nm with 84% efficiency, Opt. Lett. 39 (10) (2014) 2979–2981.
[3] F. Furrer, T. Franz, M. Berta, A. Leverrier, V. Scholz, M. Tomamichel, R. Werner, Continuous variable quantum key distribution: Finite-key analysis of composable security against coherent attacks, Phys. Rev. Lett. 109 (10) (2012) 100502.
[4] E.S. Polzik, J. Carri, H.J. Kimble, Spectroscopy with squeezed light, Phys. Rev. Lett. 68 (20) (1992) 3020.
[5] C.E. Vollmer, C. Baune, A. Samblowski, T. Eberle, V. Händchen, J. Fiurášek, R. Schnabel, Quantum up-conversion of squeezed vacuum states from 1550 to 532 nm, Phys. Rev. Lett. 112 (7) (2014) 073602.
[6] J.S. Dam, P. Tidemand-Lichtenberg, C. Psdersen, Room-temperature mid-infrared single-photon spectral imaging, Nat. Photonics 6 (2012) 788–793.
[7] J.C. Bienfang, C.A. Denman, B.W. Grime, P.D. Hillman, G.T. Moore, J.M. Telle, 20 W of continuous-wave sodium D2 resonance radiation from sum-frequency generation with injection-locked lasers, Opt. Lett. 28 (22) (2003) 2219–2221.
[8] T. Nishikawa, A. Ozawa, Y. Nishida, M. Asobe, F.L. Hong, T.W. Hansch, Efficient 494 mW sum-frequency generation of sodium resonance radiation at 589 nm by using a periodically poled Zn:$LiNbO_3$ ridge waveguide, Opt. Express 17 (20) (2009) 17792–17800.
[9] L.D. Turner, K.P. Weber, C.J. Hawthorn, R.E. Scholten, Frequency noise characterization of narrow linewidth diode lasers, Opt. Commun. 201 (4) (2002) 391–397.
[10] J.P. Qian, L. Zhang, H.W. Jiang, S.Z. Cui, J.Q. Zhou, Y. Feng, 2 w single-frequency, low-noise 509 nm laser via single-pass frequency doubling an ECDL-seeded Yb fiber amplifier, Appl. Opt. 57 (29) (2018) 8733–8737.
[11] J. Rollins, D. Ottaway, M. Zucker, R. Weiss, R. Abbott, Solid-state laser intensity stabilization at the $10^{-8}$ level, Opt. Lett. 29 (16) (2004) 1876–1878.
[12] J. Yu, Y. Qin, Z.H. Yan, H.D. Lu, X.J. Jia, Improvement of the intensity noise and frequency stabilization of Nd:YAP laser with an ultra-low expansion Fabry–Perot cavity, Opt. Express 27 (3) (2019) 3247–3254.
[13] P.S. Kuo, J.S. Pelc, O. Slattery, Y.S. Kim, M.M. Fejer, X. Tang, Reducing noise in single-photon-level frequency conversion, Opt. Lett. 38 (8) (2013) 1310–1312.
[14] M.W. Sheikhey, M. Goudarzi, R. Yadipour, H. Baghban, Analytical investigation of relative intensity noise properties of injection-locked mid-IR quantum cascade lasers, J. Opt. Soc. Amer. B 33 (11) (2016) D57–D64.
[15] A. Godard, M. Raybaut, T. Schmid, M. Lefebvre, A.M. Michel, M. Pealat, Management of thermal effects in high-repetition-rate pulsed optical parametric oscillators, Opt. Lett. 35 (21) (2010) 3667–3669.
[16] M. Sabaeian, L. Mousave, H. Nadgaran, Investigation of thermally-induced phase mismatching in continuous-wave second harmonic generation: A theoretical model, Opt. Express 18 (18) (2010) 18732–18743.
[17] X. Liu, X.J. Shen, D.M. Diao, L. Wang, Temperature-insensitive sum frequency generation of 355 nm ultraviolet laser radiation in LiB3O5 by compensating thermally induced phase mismatch, Appl. Opt. 57 (5) (2018) 1134–1139.
[18] Y. Kaneda, S. Kubota, Theoretical treatment simulation and experiments of doubly resonant sum-frequency mixing in an external resonator, Appl. Opt. 36 (30) (1997) 7766–7775.
[19] M.A. Albota, N.C. Wong, Efficient single-photon counting at 1.55μm by means of frequency upconversion, Opt. Lett. 29 (13) (2004) 1449–1451.
[20] H.F. Pan, H.F. Dong, H.P. Zeng, W. Lu, Efficient single-photon counting at 1.55 μm by intra-cavity frequency upconversion in a unidirectional ring laser, Appl. Phys. Lett. 89 (19) (2006) 191108.
[21] W. Tan, X.D. Qiu, G. Zhao, M.Y. Jia, W.G. Ma, X.J. Yan, L. Dong, L. Zhang, Z.M. Tong, W.B. Yin, X.X. Feng, L.T. Xiao, O. Axner, S.T. Jia, High-efficiency frequency upconversion of 1.5μm laser based on a doubly resonant external ring cavity with a low finesse for signal laser, Appl. Phys. B 123 (2) (2017) 52:1–9.
[22] A.P. VanDevender, P.G. Kwiat, Quantum transduction via frequency upconversion (Invited), J. Opt. Soc. Amer. B 24 (2) (2007) 295–299.
[23] K. Sugiyama, S. Kawajiri, N. Yabu, K. Matsumoto, M. Kitano, Sum-frequency mixing of radiation from two extended-cavity laser diodes using a doubly resonant external cavity for laser cooling of trapped ytterbium ions, Appl. Opt. 49 (29) (2010) 5510–5516.
[24] J.D. Vance, C.Y. She, H. Moosmüller, Continuous-wave, all-solid-state, single-frequency 400 mw source at 589 nm based on doubly resonant sum-frequency mixing in a monolithic lithium niobate resonator, Appl. Opt. 37 (21) (1998) 4891–4896.
[25] C.A. Denman, P.D. Hillman, G.T. Moore, J.M. Telle, J.E. Preston, J.D. Drummond, R.Q. Fugate, 50 W CW single frequency 589 nm FASOR, Adv. Solid-State Photonics (2005) 698–702.
[26] E. Mimoun, L.D. Sarlo, J.-J. Zondy, J. Dalibard, F. Gerbier, Sum-frequency generation of 589 nm light with near-unit efficiency, Opt. Express 16 (23) (2008) 18684–18691.
[27] D.K. Choge, H.X. Chen, L. Guo, G.W. Li, W.G. Liang, Double-pass high-efficiency sum-frequency generation of a broadband orange laser in a single MgO:PPLN crystal, Opt. Mater. Express 9 (2) (2019) 837–844.
[28] G.T. Moore, Resonant sum-frequency generation, IEEE J. Quantum Electron. 38 (1) (2002) 12–18.
[29] R.W. Boyd, Nonlinear Optics, third ed., Elsevier, New York, 2008, pp. 91–93.
[30] J.A. Armstrong, N. Bloembergen, J. Ducuing, P.S. Pershan, Interactions between light waves in a nonlinear dielectric, Phys. Rev. 127 (6) (1962) 1918–1939.